

RESEARCH LETTER

10.1002/2016GL069577

Special Section:

First results from NASA's
Magnetospheric Multiscale
(MMS) Mission

Key Points:

- A method is presented to routinely assess the ionospheric electrodynamic context of MMS magnetopause observations
- Two magnetopause crossings examined require erosion in addition to compression consistent with observed polar cap expansion
- The convection implies that MMS observations are related to the main path of flux transport in the first case but not in the second

Supporting Information:

- Supporting Information S1
- Movie S1
- Movie S2

Correspondence to:

B. J. Anderson,
brian.anderson@jhuapl.edu

Citation:

Anderson, B. J., et al. (2016),
Electrodynamic context of
magnetopause dynamics observed
by magnetospheric multiscale,
Geophys. Res. Lett., 43, 5988–5996,
doi:10.1002/2016GL069577.

Received 13 MAY 2016

Accepted 3 JUN 2016

Accepted article online 6 JUN 2016

Published online 21 JUN 2016

©2016. The Authors.

This is an open access article under the terms of the Creative Commons Attribution-NonCommercial-NoDerivs License, which permits use and distribution in any medium, provided the original work is properly cited, the use is non-commercial and no modifications or adaptations are made.

Electrodynamic context of magnetopause dynamics observed by magnetospheric multiscale

Brian J. Anderson¹, Christopher T. Russell², Robert J. Strangeway², Ferdinand Plaschke³, Werner Magnes³, David Fischer³, Haje Korth¹, Viacheslav G. Merkin¹, Robin J. Barnes¹, Colin L. Waters⁴, Ian J. Cohen¹, Joseph H. Westlake¹, Barry H. Mauk¹, Hannes K. Leinweber², Daniel J. Gershman⁵, Barbara L. Giles⁵, Guan Le⁵, Roy B. Torbert⁶, and James L. Burch⁷

¹Johns Hopkins University Applied Physics Laboratory, Laurel, Maryland, USA, ²Department of Earth, Planetary, and Space Sciences, University of California, Los Angeles, California, USA, ³Space Research Institute, Austrian Academy of Sciences, Graz, Austria, ⁴School of Mathematical and Physical Sciences, University of Newcastle, Callaghan, New South Wales, Australia, ⁵NASA Goddard Space Flight Center, Greenbelt, Maryland, USA, ⁶Institute for the Study of Earth, Oceans, and Space, University of New Hampshire, Durham, New Hampshire, USA, ⁷Southwest Research Institute, San Antonio, Texas, USA

Abstract Magnetopause observations by Magnetospheric Multiscale (MMS) and Birkeland currents observed by the Active Magnetosphere and Planetary Electrodynamic Response Experiment are used to relate magnetopause encounters to ionospheric electrodynamics. MMS magnetopause crossings on 15 August and 19 September 2015 occurred earthward of expectations due to solar wind ram pressure alone and coincided with equatorward expansion of the Birkeland currents. Magnetopause erosion, consistent with expansion of the polar cap, contributed to the magnetopause crossings. The ionospheric projections of MMS during the events and at times of the magnetopause crossings indicate that MMS observations are related to the main path of flux transport in one case but not in a second. The analysis provides a way to routinely relate in situ observations to the context of in situ convection and flux transport.

1. Introduction

A primary objective of the Magnetospheric Multiscale (MMS) mission is to understand magnetic reconnection at Earth's magnetopause and in the magnetotail [Burch *et al.*, 2015]. Launched on 12 March 2015, the mission achieves breakthrough observational capabilities with high-rate field and plasma observations and state-of-the-art navigation of the four MMS observatories [Tooley *et al.*, 2014; Fuselier *et al.*, 2014]. It is important to relate MMS observations to magnetosphere–ionosphere (MI) dynamics. Regarding the magnetosphere as a natural laboratory for the “experiments” observed by MMS, observations of ionospheric convection can establish the context specific to MMS observations. Combining observations from MMS with measures of MI dynamics allows us to understand relationships between local- and system-scale processes.

We present results for MMS magnetopause encounters on 15 August and 19 September 2015, with ionospheric electrodynamic context derived from the Active Magnetosphere and Planetary Electrodynamic Response Experiment (AMPERE) to help determine what led to the MMS magnetopause encounters and whether MMS observations were made near the primary pathway of magnetic flux transport from the dayside magnetosphere into the polar cap.

2. Data and Processing

Data used from MMS are the Flux Gate Magnetometer (FGM) [Russell *et al.*, 2014], the Fast Plasma Investigation (FPI) [Pollock *et al.*, 2016], and the Energetic Particle Detector–Energetic Ion Spectrometer (EPD–EIS) [Mauk *et al.*, 2015]. FGM returns 0.02 nT resolution measurements of the vector magnetic field at 16 (256) samples/s in survey (burst) mode. Differential measurements are enabled by MMS precision avionics and navigation systems [Tooley *et al.*, 2014]. The FPI measures 10 eV/q to 30 keV/q ions and electrons using eight energy spectrometers on each spacecraft and provides distribution functions in survey mode every 4.5 s and in burst mode every 30 ms and 150 ms for electrons and ions, respectively [Pollock *et al.*, 2016]. We use ion density, n_i , and ion temperature perpendicular, $T_{i\perp}$, and parallel, $T_{i\parallel}$, to the magnetic field. The EIS measures ~ 20 keV to >0.5 MeV ions and electrons with time-of-flight species discrimination for ions [Mauk *et al.*, 2014] and obtains 4π sr coverage every spacecraft spin (~ 20 s spin period). Electron detection

from EIS is a secondary product and was acquired from two spacecraft at a time. We use data from one sector detecting particles with pitch angles between 0° and 90° in the dayside magnetosphere.

AMPERE uses attitude magnetometer data from the Iridium satellite constellation to derive global distributions of Birkeland field-aligned currents every 10 min [Anderson *et al.*, 2000, 2002; Waters *et al.*, 2001; Anderson *et al.*, 2014]. The 66 space vehicles in the communication network are in 780 km altitude, circular, near-polar orbits, distributed over six orbit planes spaced equally in longitude, giving ~ 2 h local time spacing, and a 9 min separation along track. Processing yields maps of the horizontal perturbations, $\delta\mathbf{B}$, and radial current density, j_r , and are available from 1 January 2010 to the present.

Quantities derived from AMPERE include the following: the total current flowing through the ionosphere is calculated from j_r [Anderson *et al.*, 2014]. We use northern hemisphere total, dayside (06:00 to 18:00 magnetic local time, MLT), and nightside (18:00 to 06:00 MLT) currents denoted as I_{Total} , I_{Day} , and I_{Night} , respectively. To characterize polar cap dynamics we use the region 1 (R1) oval of Clausen *et al.* [2012], which yields the R1 latitude as a function of MLT when j_r is constrained at dawn and dusk. The area poleward of the R1 latitude is denoted A_{R1} . An equivalent ionospheric convection potential, ϕ_{eq} , and electric field magnitude, E_{eq} , are derived using the MIX electrostatic solver [Merkin and Lyon, 2010], using j_r and a uniform 8S ionospheric conductance. The equivalent convection reflects the basic features of the actual convection because the potential pattern, on the large scale, is determined by the locations and polarities of the largest electric fields which occur between adjacent upward and downward j_r [Richmond and Thayer, 2000; Marsal *et al.*, 2012]. To estimate the MMS foot point, we use the T96 [Tsyganenko, 1995] model, with nominal model parameters $D_{\text{st}} = -20$ nT, solar wind pressure (P_{Ram}) of 3 nPa, and zero interplanetary magnetic field (IMF) to trace from the MMS location to 130 km altitude in the northern hemisphere.

3. Case 1: 15 August 2015

Figure 1a shows MMS3 data for 10:10 to 11:50 UT on 15 August 2015 at the beginning of a moderate geomagnetic storm. FPI data were not returned for this interval. A magnetopause crossing (MP) occurred from 11:04 to 11:09 UT as evidenced by negative turning of B_z , the maximum $J_T = |\mathbf{J}|$, and decreases in the energetic electron and ion count rates. This time period was used to identify the magnetopause normal by minimum variance analysis, $\mathbf{n}_{\text{MP}} = (0.787, 0.367, -0.496)$ in GSM. The current density was rotated into LMN coordinates [cf. Song and Russell, 1999], and J_T and J_M are shown. From 10:42 to 11:03 UT the magnetic field was variable, J_T exceeded $0.3 \mu\text{A}/\text{m}^2$, and the electron count rate decreased relative to levels prior to 10:42 UT but without a corresponding decrease in the proton count rate. Since B_z did not reverse sign, we interpret these signatures to indicate residence in the low-latitude boundary layer.

For this interval, during late commissioning, the minimum, average, and maximum MMS separations were 161, 232, and 299 km, respectively. The tetrahedron quality factor, Q_v [Fuselier *et al.*, 2014], was 0.73. The finite difference divergence of \mathbf{B} , $\text{div}(\mathbf{B})$, in current density units, gave an average $|\text{div}(\mathbf{B})|$ from 10:41 to 11:10 UT of $0.032 \mu\text{A}/\text{m}^2$. The average J_T was $0.084 \mu\text{A}/\text{m}^2$, indicating that the current density is uncertain to $\sim 40\%$.

Figure 1b shows the AMPERE $\delta\mathbf{B}$, j_r , and ϕ_{eq} for 10:50 to 11:00 UT. The “spiral” form of the dawn R1 to dusk region 2 (R2) downward current [Korth *et al.*, 2010] is consistent with an IMF clock angle between 90° and 180° as observed (cf. Figure 2). In the north, this corresponds to convection into the polar cap from dusk across noon from magnetopause reconnection in the afternoon. The MMS foot point is near the maximum E_{eq} .

Figure 2 shows the solar wind and IMF parameters together with the measures of ionospheric electrodynamic derived from AMPERE. Increases in A_{R1} indicate greater open magnetic flux, which implies transport of magnetic flux from the dayside magnetosphere into the polar cap and should correspond to earthward displacement of the magnetopause due to erosion. We evaluated the arc length at 130 km altitude between the locations of $\phi_{\text{eq-min}}$ and $\phi_{\text{eq-max}}$, denoted as dS_ϕ , to obtain a mean electric field magnitude, $E_{\text{PC}} = \Delta\phi_{\text{eq}}/dS_\phi$. For the solar wind and IMF, we show values calculated from the OMNI data as well as values from Advanced Composition Explorer (ACE) data advected to Earth using the average OMNI delay time.

The MP crossing occurred when MMS3 was at $8.3 R_E$ ($R_E = 6371$ km, Earth’s mean radius), geocentric distance, and 16.4 MLT. An interplanetary shock arrived at Earth shortly after 08:30 UT (cf. Figure 2), and P_{Ram} increased from ~ 2 nPa to ~ 6 nPa, with subsequent variations, and increased again from ~ 5 nPa to ~ 10 nPa near 11:00 UT.

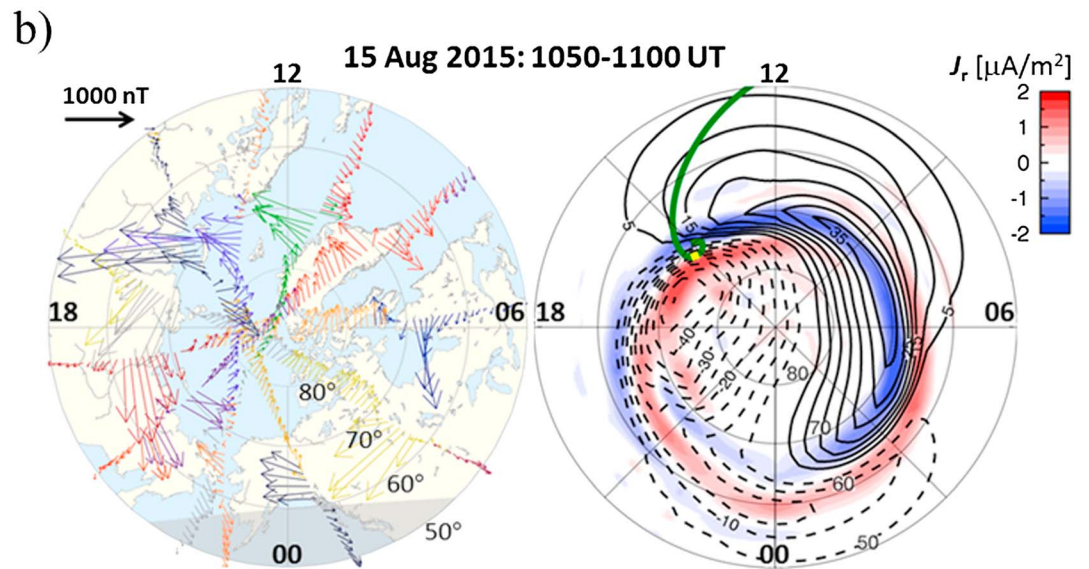
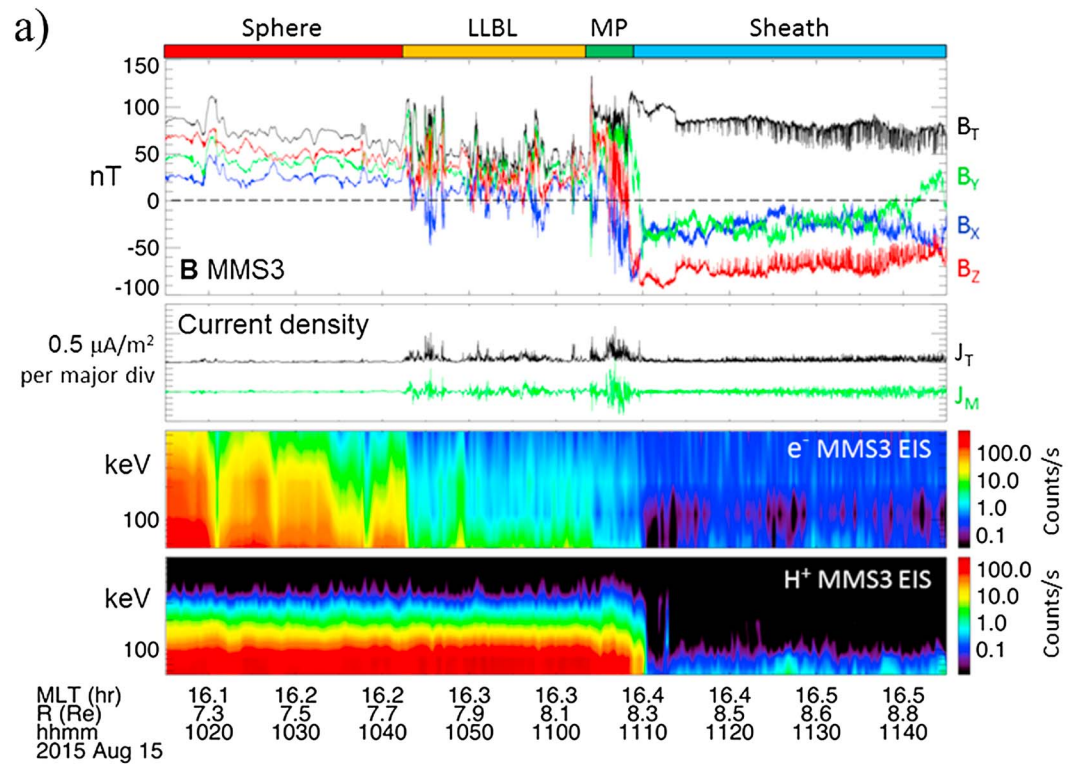


Figure 1. (a) Magnetic field and particle data from MMS on 15 August 2015 for the magnetopause crossing at 10:50 to 11:00 UT and (b, left) AMPERE horizontal $\delta\mathbf{B}$ and (right) j_r and ϕ_{eq} for the magnetopause crossing. From the top in Figure 1a, the plots show the regions identified from the data; MMS3 FGM data in GSM coordinates (colored traces) and the total field (black trace); current density calculated from the four MMS FGM data [cf. De Keyser *et al.*, 2005], showing J_T (black) and J_M (green); electron count rate (50 to 650 keV); and proton count rate (50 to 800 keV). AMPERE $\delta\mathbf{B}$ for each satellite are shown using different colored arrows originating at the satellite location, scaled as indicated. Positive j_r in red are upward and negative j_r in blue are downward. Positive and negative ϕ_{eq} are solid and dashed contours, respectively. The green curve is the MMS footprint from 06:00 to 15:00 UT, and the yellow dot indicates the MMS footprint at 10:55 UT.

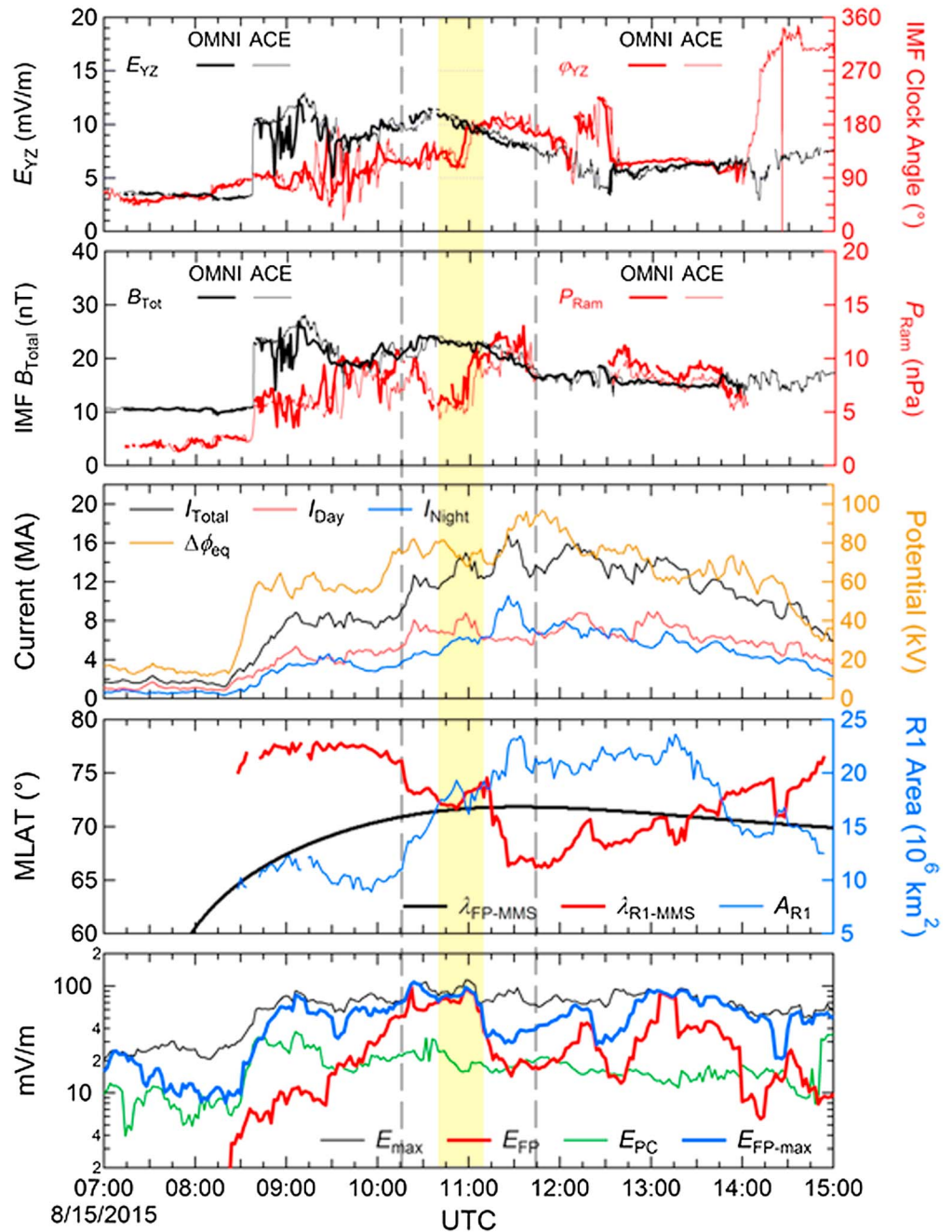


Figure 2. Solar wind and interplanetary parameters together with electrodynamic quantities derived from AMPERE j_r for 07:00 to 15:00 UT on 15 August 2015. Vertical dashed lines show the time span of data in Figure 1, and gold shading indicates the MMS magnetopause crossing. From the top, the plots show the solar wind electric field magnitude in the y-z GSM plane, $E_{yz} = |V_x|(B_y^2 + B_z^2)$; IMF clock angle, $\phi_{IMF} = \text{atan2}(B_y, B_z)$; IMF magnitude, B_{Total} ; P_{Ram} ; northern total currents and equivalent potential drop, $\Delta\phi_{eq} = \phi_{eq-max} - \phi_{eq-min}$; magnetic latitude of the MMS foot point, λ_{FP-MMS} ; R1 oval latitude at the MMS foot point local time, λ_{R1-MMS} ; total area within the R1 oval, A_{R1} ; maximum E_{eq} , E_{max} ; E_{eq} at the MMS foot point, E_{FP} ; and the maximum E_{eq} at the MMS foot point local time, E_{FP-max} . In the top two plots, thick (thin) traces are the OMNI results (advected ACE data).

To examine the contribution of erosion to the observed MP location, we evaluated the *Shue et al.* [1998] model magnetopause at the MMS3 local time using P_{Ram} and IMF B_z from the OMNI (ACE) data averaged for 20 min after the P_{Ram} increase near 11:00 UT, which give $P_{Ram} = 10.6$ nPa (9.0 nPa) and $B_z = -19.6$ nT (-20.3 nT). With $B_z = 0$, the OMNI (ACE) radial distance of the MP is 9.9 (10.1) R_E , whereas using the measured

B_z gives the MP at 8.2 (8.4) R_E . This indicates that erosion contributed significantly to displacing the MP earthward.

To assess whether MMS was located in regions of strong convection, we compared E_{\max} and E_{PC} to E_{FP} and $E_{FP-\max}$. If E_{FP} and $E_{FP-\max}$ are near E_{\max} , this indicates that MMS observations were made on field lines linked to the driver of ionospheric convection. If E_{FP} and $E_{FP-\max}$ are lower than E_{PC} , then the MMS observations were likely not linked to primary MI forcing. If they are between E_{\max} and E_{PC} and the foot point local time is on the dayside between the extrema in ϕ_{eq} , then it is likely that the field threading MMS was contributing to dayside convection into the polar cap.

Activity onset coincided with the shock arrival near 08:20 UT as indicated by jumps in E_{yz} , B_{Total} , and P_{Ram} and increases in $\Delta\phi_{eq}$, I_{Total} , and A_{R1} . The IMF turned very slightly southward and was variable but predominantly duskward, ϕ_{IMF} between 90° and 150° . With the increased currents, the R1 oval fit returned results as indicated by the traces for λ_{R1-MMS} and A_{R1} . Until $\sim 10:15$ UT, λ_{R1-MMS} was above 75° while A_{R1} was 10 to 12 $M km^2$. Even though P_{Ram} increased to ~ 10 nPa from 09:15 to 09:30 UT, I_{Tot} and A_{R1} do not increase further until 10:15 UT, after the IMF turned further southward, $\phi_{IMF} \sim 150^\circ$. P_{Ram} dropped to ~ 6 nPa near 10:50 UT, but I_{Tot} and A_{R1} continued to increase. Near 11:00 UT the IMF turned more southward, $\phi_{IMF} \sim 180^\circ$, and P_{Ram} increased to ~ 9 nPa. Shortly thereafter, λ_{R1-MMS} decreased by $\sim 5^\circ$ and A_{R1} nearly doubled to over 20 $M km^2$. The increase in A_{R1} confirms the addition of magnetic flux to the polar cap. Subsequently, E_{yz} gradually decreased while ϕ_{IMF} varied between 150° and 180° and became steady near 130° starting $\sim 12:30$ UT, while A_{R1} remained near 20 $M km^2$ and the total current varied between 12 and 16 MA.

The MMS spacecraft were outbound, and λ_{FP-MMS} increased from under 60° to over 70° by 10:00 UT. In addition, E_{\max} increased starting at 08:30 UT from just over 30 mV/m to near 70 mV/m by 09:00 UT, while E_{PC} increased from about 10 mV/m to near 30 mV/m with the arrival of the shock and the increase in E_{yz} from ~ 4 mV/m to over 10 mV/m. Initially, E_{FP} was below E_{PC} but it increased starting at 08:30 UT and exceeded E_{PC} at $\sim 09:30$ UT. By 09:00 UT, $E_{FP-\max}$ increased to just under E_{\max} , indicating that MMS was in the same local time sector as the strongest convection.

From 09:00 to 10:00 UT, λ_{FP-MMS} increased as the spacecraft continued outbound, and E_{FP} increased steadily from near E_{PC} to just under E_{\max} . Between 09:00 and 11:00 UT $E_{FP-\max}$ remained very close to E_{\max} . At about 10:15 UT, there was a fairly sharp reduction in λ_{R1-MMS} to within 2° of the MMS foot point and A_{R1} increased to about 19 $M km^2$. The MMS magnetopause crossing occurred as the polar cap expanded over the MMS foot point, suggesting that the polar cap expansion, driven by transport of flux from the dayside magnetosphere, played a significant role in bringing the magnetopause earthward. At the time of the magnetopause crossing, both E_{FP} and $E_{FP-\max}$ were close to E_{\max} , implying that MMS was located on field lines connected to the primary driver of convection.

After 11:10 UT, there is a further equatorward expansion of the Birkeland currents and λ_{R1-MMS} reached a minimum latitude of just over 65° latitude, $\sim 5^\circ$ equatorward of λ_{FP-MMS} . At the same time, A_{R1} reached a maximum of about 23 $M km^2$, while E_{FP} and $E_{FP-\max}$ decreased, suggesting that the peak in the convection moved away from the MMS local time. This is consistent with the nearly purely southward IMF and the Birkeland current and ϕ_{eq} patterns (cf. Movie S1 in the supporting information), which show that a two-cell convection pattern formed; such that, the MMS foot point local time remained in the region of antisunward convection but within a much broader convection throat into the polar cap. At this time, the highest E_{eq} occurred between the R1 and R2 currents near dawn and dusk, associated with return convection within the magnetosphere. After about 12:10 UT, λ_{R1-MMS} gradually increased. Except for an interval near 13:00 UT when the oval retreated to the MMS foot point latitude, until $\sim 13:30$ UT, λ_{R1-MMS} remained steadily lower than λ_{FP-MMS} and the R1 oval remained expanded, with an area of ~ 20 $M km^2$. At $\sim 13:30$ UT, the oval size decreased and λ_{R1-MMS} crossed poleward of the MMS foot point, indicating retreat of the polar cap and expansion of the magnetopause outward. Consistent with these dynamics, the MMS spacecraft were resident close to the magnetopause from about 12:50 UT to 13:15 UT and crossed into the magnetosphere near 13:50 UT to 14:10 UT (cf. Figure S1 in the supporting information). We note that P_{Ram} appears to be gradually decreasing from 12:30 to 14:00 UT as well, although the decrease in P_{Ram} at 10:15 UT seemed to have no effect on A_{R1} or λ_{R1-MMS} .

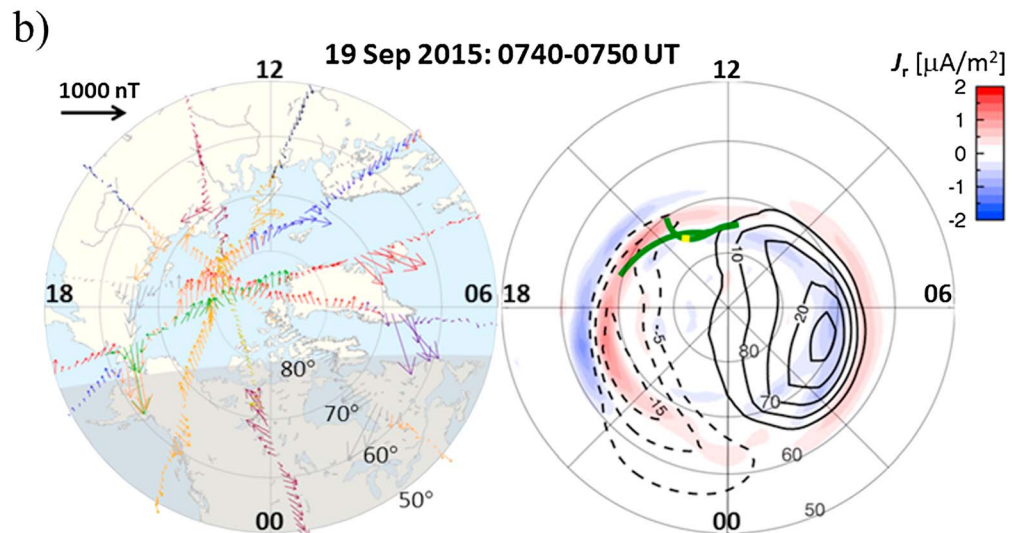
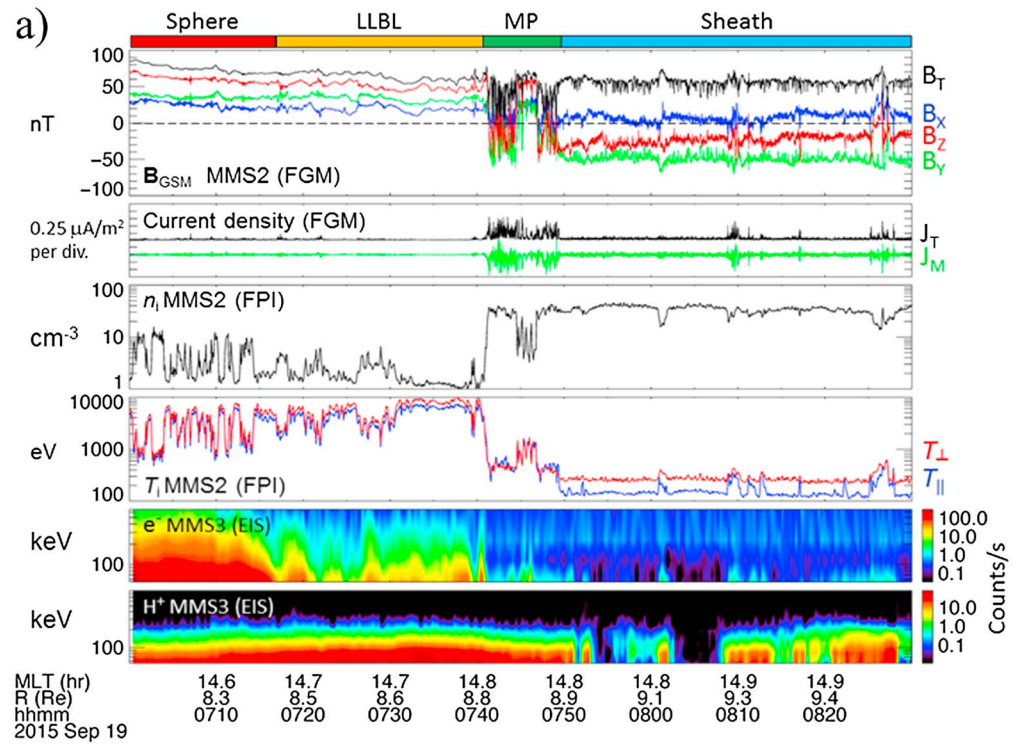


Figure 3. (a) Magnetic field and particle data from MMS2 on 19 September 2015 for the magnetopause crossing at 07:40 to 07:50 UT and (b, left) AMPERE horizontal $\delta\mathbf{B}$ and (right) J_r and φ_{eq} for the magnetopause crossing. The top two plots and the bottom two plots are in the same format as Figure 1a. The middle two plots show the plasma ion density, n_i , in the third plot, and temperature moments (perpendicular $T_{i\perp}$, in red, and parallel $T_{i\parallel}$, in blue) in the fourth plot.

4. Case 2: 19 September 2015

Data for a second magnetopause crossing are shown in Figure 3 together with the AMPERE data. For this case, FPI data are available and n_i and $T_{i\perp}$ and $T_{i\parallel}$ are shown in the middle plots. The magnetopause crossing occurred from 07:41 to 07:49 UT as reflected in the reversals of B_y and B_z , a decrease in energetic electron counts, and a transition from hot/tenuous plasma to cooler/dense plasma. The relative increase in density is nearly the same as the decrease in temperature so that the ion thermal pressure is similar inside and outside the magnetopause.

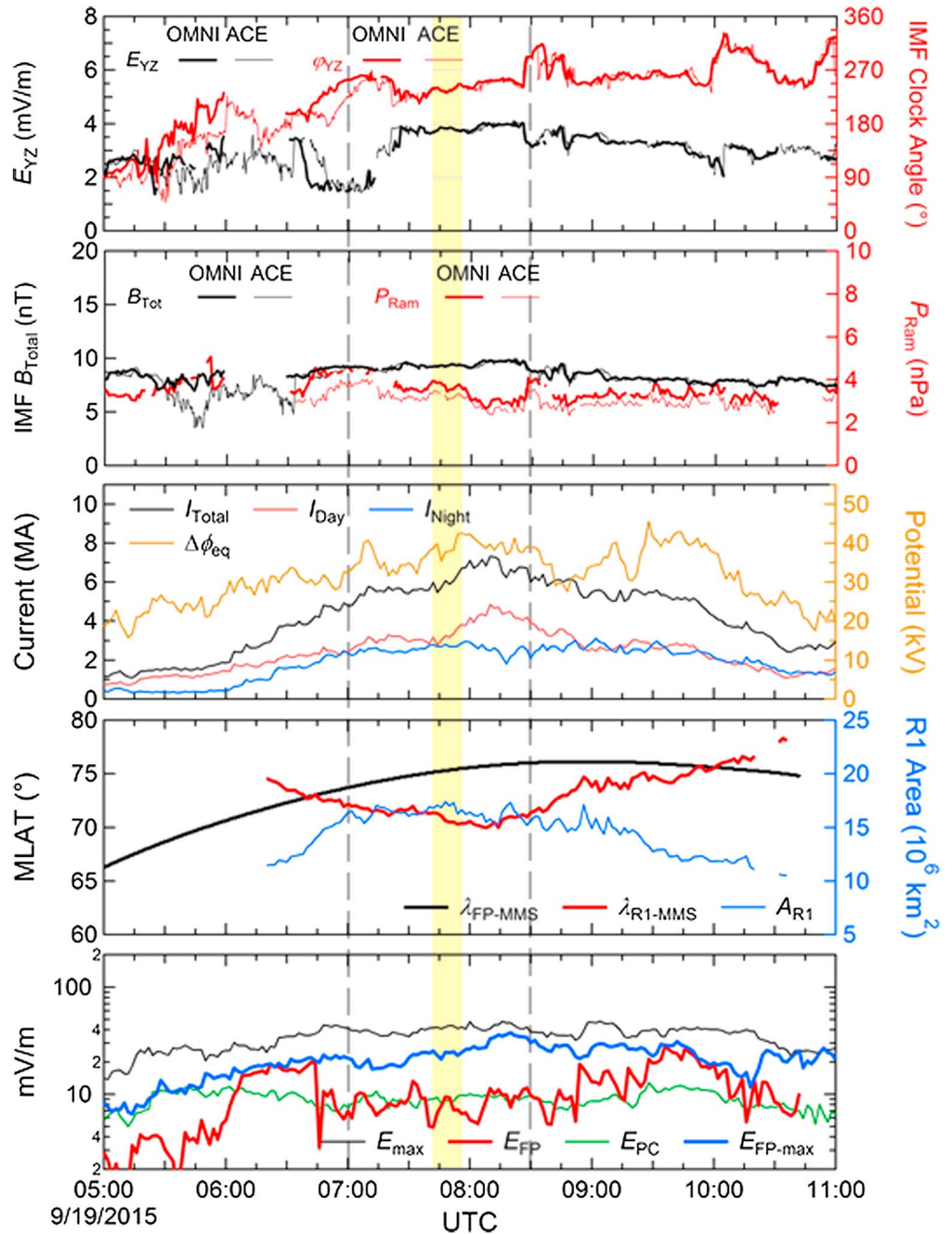


Figure 4. Solar wind and interplanetary parameters together with electrodynamic quantities derived from AMPERE j_r for 05:00 to 11:00 UT on 19 September 2015 in the same format as in Figure 2.

The minimum, average, and maximum MMS observatory separations were 48, 72, and 90 km, respectively, and Q_v was 0.78. The average $|div(\mathbf{B})|$ from 07:40 to 07:50 UT was $0.065 \mu\text{A}/\text{m}^2$, whereas the average J_T was $0.21 \mu\text{A}/\text{m}^2$. At this local time, 14.8 MLT, the observed magnetopause distance was $8.8 R_E$. The EPD electron counts drop substantially at 07:40 UT when n_i increases from $\sim 1 \text{ cm}^{-3}$ to $\sim 30 \text{ cm}^{-3}$ and $T_{\perp L}$ decreases from $\sim 9 \text{ keV}$ to $\sim 400 \text{ eV}$ associated with the first reversals in B_z and B_y . A brief crossing back to the magnetospheric side of the current layer occurred from 07:44 to 07:47 UT, which is reflected in intermediate values of n_i and $T_{\perp L}$. The EPD proton counts remained fairly high except for two periods near 07:56–07:58 UT and 08:03–08:09 UT. The sustained proton count rate suggests that MMS2 remained relatively close to the magnetopause. Later in the orbit, from $\sim 08:40$ to 13:00 UT, the magnetopause

crossed over the MMS2 multiple times, while the energetic proton counts remained generally near their magnetospheric levels and the energetic electrons exhibited count rates similar to those near 07:45 UT in Figure 3 (Figure S2).

The AMPERE j_r shows R1 currents just poleward of 70° magnetic latitude in the vicinity of the MMS foot point at 07:45 UT (Figure 3b). The time development is shown in Figure 4 (and image frames in Movie S2). The Birkeland currents are more symmetric dawn-to-dusk than for case 1, but the upward current extends across noon from the dusk R1 currents to the dawn R2 currents, consistent with a negative IMF B_y component, ϕ_{IMF} between 180° and 270°. The IMF is duskward at 05:00 UT and turns southward shortly before 05:30 UT and turns toward dawn, negative B_y but still southward, $\phi_{\text{IMF}} \sim 210^\circ$, at about 06:45 UT, where it remains until about 08:30 UT when it turns slightly northward. From 05:00 to 06:45 UT, E_{yz} is variable between 1.5 and 3 mV/m until 07:15 UT when it rises from 1.5 mV/m to 4 mV/m. There is no shock during this event, and P_{Ram} decreases with some variability from ~ 4 nPa to just over 3 nPa. The average P_{Ram} and IMF B_z from OMNI (ACE) from 07:30 to 07:50 UT were 3.7 nPa (3.2 nPa) and -5.5 nT (-5.8 nT); such that, the Shue *et al.* [1998] MP distance at this local time would be $10.2 R_E$ ($10.4 R_E$) with $B_z = 0$ and $9.7 R_E$ ($9.8 R_E$) with the measured IMF B_z . The observed MP was therefore almost $1.5 R_E$ earthward of the model estimate based on P_{Ram} alone and still $1.0 R_E$ inside the model estimate including the IMF B_z .

The Birkeland currents increase near 06:00 UT possibly in response to the southward IMF rotation. By 07:00 UT, I_{Total} rose to ~ 5 MA, while $\Delta\phi_{\text{eq}}$ increased to ~ 30 kV. The maximum $\Delta\phi_{\text{eq}}$ over the entire interval was ~ 40 kV. R1 oval fits were obtained from 06:20 UT to 10:15 UT and show first an equatorward expansion with $\lambda_{\text{R1-MMS}}$ reaching $\sim 69^\circ$ MLT just after 08:00 UT and then a retreat poleward with $\lambda_{\text{R1-MMS}} \sim 76^\circ$ by 10:15 UT. Correspondingly, A_{R1} increased from ~ 10 M km² at 06:20 UT to ~ 16 M km² by 07:00 UT and remained there until $\sim 09:00$ UT. The variations of A_{R1} and $\lambda_{\text{R1-MMS}}$ are not due to an increase in P_{Ram} . The AMPERE results confirm that the MMS magnetopause encounter occurred during a period of polar cap expansion. The expansion is more modest than in case 1, but $\lambda_{\text{FP-MMS}}$ is higher because the MMS orbit apogee is closer to noon, and $\lambda_{\text{FP-MMS}}$ is poleward of $\lambda_{\text{R1-MMS}}$ when the magnetopause crossing occurred and throughout 06:45 to 10:00 UT, which we attribute to mapping uncertainties.

The equivalent convection electric fields are lower in this case, with E_{max} never exceeding about 40 mV/m. In addition, E_{FP} and $E_{\text{FP-max}}$ are lower relative to E_{max} and E_{PC} than for case 1. $E_{\text{FP-max}}$ is ~ 5 to 10 mV/m lower than E_{max} but closer to E_{max} than to E_{PC} , while E_{FP} is generally close to or below E_{PC} . That the foot point mappings would have indicated a magnetopause crossing rather earlier than observed suggests that $E_{\text{FP-max}}$ is probably a better indicator of E_{eq} in the vicinity of the actual MMS foot point. The morning convection cell is stronger so that MMS is not situated in the local time sector of strongest flow into the polar cap. Perhaps reflecting this, while substantially greater than E_{PC} , $E_{\text{FP-max}}$ is lower than E_{max} . Thus, while the MMS foot point local time is in the region of antisunward convection into the polar cap, it is not in the local time of strongest antisunward convection.

5. Discussion and Conclusions

Ionospheric electrodynamics observed during MMS magnetopause crossings provide context for interpreting MMS observations both by helping to identify the processes causing the magnetopause crossing and by locating the MMS observations in MI convection. We show two cases in which MMS magnetopause crossings occurred during polar cap expansion and enhanced dayside convection. In these cases, the MMS magnetopause crossings occurred inside the predicted magnetopause given solar wind ram pressure alone. We suggest that this was due to erosion of the dayside magnetosphere in consequence of magnetic reconnection [Aubry *et al.*, 1970; cf. Le *et al.*, 2016]. Erosion has been interpreted as a consequence of flux transport into the polar cap or as a result of intense R1 currents [cf. Sibeck *et al.*, 1991]; both of which occurred in concert with the MMS magnetopause crossings. The results illustrate that observations of ionospheric electrodynamics can assist in specifying the actual response of the MI system.

Mapping the MMS location to the ionospheric foot point provides a means to place the in situ observations in the context of convection. For the 15 August 2015 case, from 10:50 to 11:00 UT, the MMS foot point was close to the region of strong convection into the polar cap, from dusk to dawn, so that MMS was well positioned in local time to observe the primary driver of convection. This is consistent with observations of the detailed

signatures of energetic particle transport for this event, which require a normal component of the magnetic field at the magnetopause [cf. *Cohen et al.*, 2015]. In the second case, 19 September 2015 from 07:40 to 07:50 UT, the MMS foot point was situated within but on the dusk side of the region of antisunward convection into the polar cap. Thus, while MMS was positioned to observe phenomena contributing to flux transport into the polar cap, it was not in the local time sector hosting the strongest convection flows. For case 2, the mapped latitude at the time of the magnetopause crossing was poleward of the R1 oval latitude, suggesting that more quantitative comparative analyses between MMS in situ observations and ionospheric electrodynamics could benefit from refinements in the mapping.

The context provided by the analyses presented here is complementary to the in situ MMS observations, which diagnose the proximity of the MMS spacecraft to the reconnection line and ion/electron diffusion regions. Applying these methods to cases in which the MMS observations indicate direct sampling of magnetic diffusion regions [cf. *Burch et al.*, 2016] is particularly attractive to establish the links between local and global dynamics. Within this context, it will be important to include observations of ionospheric flows to compare the in situ flows and fields to reliable measures of the ionospheric electric fields.

Acknowledgments

The dedication and expertise of the MMS development and operations teams are greatly appreciated. Work at JHU/APL, UCLA, UNH, GSFC, and SwRI was supported by NASA contract NNG04EB99C. As of 1 March 2016, MMS data are available for 1 September 2015 to 31 January 2016 from the MMS Science Data Center website: <https://lasp.colorado.edu/mms/sdc/>. Data for 15 August 2015 are available upon request. The sources for interplanetary magnetic field and solar wind plasma data, Advanced Composition Explorer (ACE) and Wind, are gratefully acknowledged. These are available through the Coordinated Data Analysis Web at http://cdaweb.gsfc.nasa.gov/cdaweb/istp_public/. Information on NASA OMNI interplanetary data sources and processing is available at ftp://spdf.gsfc.nasa.gov/pub/data/omni/high_res_omni/. AMPERE development, data acquisition, and science processing were supported by NSF awards ATM-0739864 and ATM-1420184 to JHU/APL, and these data are available via the AMPERE Science Data Center website: <http://ampere.jhuapl.edu>. Support for Anderson and Korth in analysis of dynamics of Birkeland currents was also provided by NASA Heliophysics Supporting Research grant NNX14AF82G.

References

- Anderson, B. J., K. Takahashi, and B. A. Toth (2000), Sensing global Birkeland currents with Iridium® engineering magnetometer data, *Geophys. Res. Lett.*, *27*, 4045–4048, doi:10.1029/2000GL000094.
- Anderson, B. J., K. Takahashi, T. Kamei, C. L. Waters, and B. A. Toth (2002), Birkeland current system key parameters derived from Iridium observations: Method and initial validation results, *J. Geophys. Res.*, *107*(A6, 1079), doi:10.1029/2001JA000080.
- Anderson, B. J., H. Korth, C. L. Waters, D. L. Green, V. G. Merkin, R. J. Barnes, and L. P. Dyrud (2014), Development of large-scale Birkeland currents determined from the Active Magnetosphere and Planetary Electrodynamics Response Experiment, *Geophys. Res. Lett.*, *41*, 3017–3025, doi:10.1002/2014GL059941.
- Aubry, M. P., C. T. Russell, and M. G. Kivelson (1970), Inward motion of the magnetopause before a substorm, *J. Geophys. Res.*, *75*, 7018–7031, doi:10.1029/JA075i034p07018.
- Burch, J. L., T. E. Moore, R. B. Torbert, and B. L. Giles (2015), Magnetospheric Multiscale overview and science objectives, *Space Sci. Rev.*, doi:10.1007/s11214-015-0164-9.
- Burch, J. L., et al. (2016), Electron-scale measurements of magnetic reconnection in space, *Science*, doi:10.1126/science.aaf2939, in press.
- Clausen, L. B. N., J. B. H. Baker, J. M. Ruohoniemi, S. E. Milan, and B. J. Anderson (2012), Dynamics of the Region 1 Birkeland current oval derived from the Active Magnetosphere and Planetary Electrodynamics Response Experiment (AMPERE), *J. Geophys. Res.*, *117*, A06233, doi:10.1029/2012JA017666.
- Cohen, I. J., et al. (2015), Early results on energetic particle dynamics and structure from the Energetic Ion Spectrometer (EIS) on the Magnetospheric Multiscale (MMS) mission, *AGU Fall Meeting*, SM51A-2546, 18 December.
- De Keyser, J., M. W. Dunlop, C. J. Owen, B. U. Ö. Sonnerup, S. E. Haaland, A. Vaivads, G. Paschmann, R. Lundin, and L. Rezeau (2005), Magnetopause and boundary layer, *Space Sci. Rev.*, *118*(1–4), 231–320, doi:10.1007/s11214-005-3834-1.
- Fuselier, S. A., W. S. Lewis, C. Schiff, R. Ergun, J. L. Burch, S. M. Petrinc, and K. J. Trattner (2014), Magnetospheric Multiscale Science Mission Profile and Operations, *Space Sci. Rev.*, doi:10.1007/s11214-014-0087-x.
- Korth, H., B. J. Anderson, and C. L. Waters (2010), Statistical analysis of the dependence of large-scale Birkeland currents on solar wind parameters, *Ann. Geophys.*, *28*, 515–530, doi:10.5194/angeo-28-515-2010.
- Le, G., et al. (2016), Magnetopause erosion during the March 17, 2015, magnetic storms: Combined field-aligned currents, auroral oval, and magnetopause observations, *Geophys. Res. Lett.*, *43*, 2396–2404, doi:10.1002/2016GL068257.
- Marsal, S., A. D. Richmond, A. Maute, and B. J. Anderson (2012), Forcing the TIEGCM model with Birkeland currents from the active magnetosphere and planetary electrodynamics response experiment, *J. Geophys. Res.*, *117*, A06308, doi:10.1029/2011JA017416.
- Mauk, B. H., et al. (2014), The Energetic Particle Detector (EPD) investigation and the Energetic Ion Spectrometer (EIS) for the Magnetospheric Multiscale (MMS) mission, *Space Sci. Rev.*, doi:10.1007/s11214-014-0055-5.
- Merkin, V. G., and J. G. Lyon (2010), Effects of the low-latitude ionospheric boundary condition on the global magnetosphere, *J. Geophys. Res.*, *115*, A10202, doi:10.1029/2010JA015461.
- Pollock, C., et al. (2016), Fast plasma investigation for Magnetospheric Multiscale, *Space Sci. Rev.*, *199*, 331–406, doi:10.1007/s11214-016-0245-4.
- Richmond, A. D., and J. P. Thayer (2000), Ionospheric dynamics: A tutorial, in *Magnetospheric Current Systems*, *Geophys. Monogr.*, vol. 118, edited by S. Ohtani et al., AGU, Washington, D. C.
- Russell, C. T., et al. (2014), The Magnetospheric Multiscale magnetometers, *Space Sci. Rev.*, doi:10.1007/s11214-014-0057-3.
- Shue, J.-H., et al. (1998), Magnetopause location under extreme solar wind conditions, *J. Geophys. Res.*, *103*, 17,691–17,700, doi:10.1029/98JA01103.
- Sibeck, D. G., R. E. Lopez, and E. C. Roelof (1991), Solar wind control of the magnetopause shape, location, and motion, *J. Geophys. Res.*, *96*, 5489–5495, doi:10.1029/90JA02464.
- Song, P., and C. T. Russell (1999), Time series data analyses in space physics, *Space Sci. Rev.*, *87*, 387–463, doi:10.1023/A:1005035800454.
- Tooley, C. R., R. K. Black, B. P. Robertson, J. M. Stone, S. E. Pope, and G. T. Davis (2014), The Magnetospheric Multiscale constellation, *Space Sci. Rev.*, doi:10.1007/s11214-015-0220-5.
- Tsyganenko, N. A. (1995), Modeling the Earth's magnetospheric magnetic field confined within a realistic magnetopause, *J. Geophys. Res.*, *100*(A4), 5599–5612, doi:10.1029/94JA03193.
- Waters, C. L., B. J. Anderson, and K. Liou (2001), Estimation of global field aligned currents using Iridium magnetometer data, *Geophys. Res. Lett.*, *28*, 2165–2168, doi:10.1029/2000GL012725.